AIAA 40th Joint Propulsion Conference
Broward County Convention Center
Fort Lauderdale, Florida
11 – 14 July 2004

AIAA-2004-3373

A MODEL FOR THERMAL DECOMPOSITION OF HYDROGEN PEROXIDE

Heister, S. D.[†], Anderson, W.E.[#], Corpening, J. H.[*]
School of Aeronautics and Astronautics, Purdue University
West Lafayette, IN 47906
and
Austin, B. L.[°]
InSpace, LLC.
West Lafayette, IN 47906

Abstract

A one-dimensional model has been developed to investigate the thermal decomposition of rocket grade hydrogen peroxide (HP) in a stream of previously decomposed HP products. The model developed assumes steady, one-dimensional adiabatic flow and includes basic mass balances, droplet evaporation, gas-phase decomposition kinetics, droplet dynamics, and control volume conservation laws. The code is adjustable for HP percent concentration for both main and secondary flows, massflow rates for both flows, and initial temperature of each. Results are shown to be consistent with prior experimental measurements. Parametric studies are presented to assess the effects of initial droplet size, secondary injectant flow, mass velocity in the primary stream, peroxide concentration, and initial liquid temperature on the decomposition process. In general, results indicate unacceptably-long decomposition distances assuming 90% HP decomposition products in the primary stream. Using 98% HP showed some improvement due to the enhanced decomposition temperature of this fluid as compared to 90% HP.

Nomenclature

A	Duct x-sectional area
C_p	Spec. heat of mixture $=C_{pv}y_v + C_{pp}y_p$
C_{HP}	Peroxide vapor concentration
D_d	Drop diameter
H	Enthalpy
h_v	Heat of vaporization
h_{rxn}	Heat of reaction
K	Unimolecular rate $=A_o e^{-Ea/RuT}$
Ea	Activation energy
Ao	Frequency factor
$\dot{m}$	Total gas flow
$\dot{m}_v$	Vapor flow rate from evaporation
P	Pressure
T	Temperature of mix
T_{sat}	Saturation temperature of HP
V	Velocity of gases
v_l	Velocity of droplets
$\dot{m}_l$	Local liquid flow rate
x	Axial distance
?	Density

Introduction

High concentration or "rocket grade" hydrogen peroxide has received increased attention for storable oxidizer applications in recent years due to its relative ease of use and low toxicity. The monopropellant characteristics of this fluid also provide unique advantages in many applications and permit the use of decomposition products for power generation or for use in "staged" bipropellant systems. Catalyst beds using silver screens or other catalytic material are frequently utilized to initiate decomposition of the fluid. However, the catalyst beds become quite bulky in higher massflow applications and there is an interest in a separate injection of liquid peroxide downstream of a catalyst bed exhaust in order to minimize system mass. In this concept, the aft-injected liquid would undergo evaporation and thermal decomposition of the hydrogen peroxide vapor evolved in this process. The focus of the present study is to develop a one-dimensional model that permits analysis of this process under arbitrary injection and catalyst bed exhaust conditions. The following
section

[†] Professor, Associate Fellow AIAA
[#] Assistant Professor, Member AIAA
[*] Graduate Student, Student Member AIAA
[°] General Manager, Member AIAA

Report Documentation Page

Form Approved
OMB No. 0704-0188

1. REPORT DATE	2. REPORT TYPE	3. DATES COVERED
07 JUN 2004		-

4. TITLE AND SUBTITLE	5a. CONTRACT NUMBER
A Model for Thermal Decomposition of Hydrogen Peroxide	**F04611-03-M-3207**
	5b. GRANT NUMBER
	5c. PROGRAM ELEMENT NUMBER

6. AUTHOR(S)	5d. PROJECT NUMBER
S Heister; W Anderson; J Corpening; B Austin	**BMSB**
	5e. TASK NUMBER **R3JK**
	5f. WORK UNIT NUMBER **BMSBR3JK**

7. PERFORMING ORGANIZATION NAME(S) AND ADDRESS(ES)	8. PERFORMING ORGANIZATION REPORT NUMBER
AFRL/PRS,5 Pollux Drive,Edwards AFB,CA,93524-7048	

9. SPONSORING/MONITORING AGENCY NAME(S) AND ADDRESS(ES)	10. SPONSOR/MONITOR'S ACRONYM(S)
	11. SPONSOR/MONITOR'S REPORT NUMBER(S)

12. DISTRIBUTION/AVAILABILITY STATEMENT
Approved for public release; distribution unlimited

13. SUPPLEMENTARY NOTES

14. ABSTRACT

A one-dimensional model has been developed to investigate the thermal decomposition of rocket grade hydrogen peroxide (HP) in a stream of previously decomposed HP products. The model developed assumes steady, one-dimensional adiabatic flow and includes basic mass balances, droplet evaporation, gas-phase decomposition kinetics, droplet dynamics, and control volume conservation laws. The code is adjustable for HP percent concentration for both main and secondary flows, massflow rates for both flows, and initial temperature of each. Results are shown to be consistent with prior experimental measurements. Parametric studies are presented to assess the effects of initial droplet size, secondary injectant flow, mass velocity in the primary stream, peroxide concentration, and initial liquid temperature on the decomposition process. In general, results indicate unacceptably-long decomposition distances assuming 90% HP decomposition products in the primary stream. Using 98% HP showed some improvement due to the enhanced decomposition temperature of this fluid as compared to 90% HP.

15. SUBJECT TERMS

16. SECURITY CLASSIFICATION OF:			17. LIMITATION OF ABSTRACT	18. NUMBER OF PAGES	19a. NAME OF RESPONSIBLE PERSON
a. REPORT	b. ABSTRACT	c. THIS PAGE			
unclassified	**unclassified**	**unclassified**		**18**	

provides a description of the model elements; results are then provided for a variety of flow conditions.

Model Development

We presume a steady, one-dimensional adiabatic flow for the purposes of the study. Figure 1 introduces some of the relevant variables in the problem; the remainder of the variables are highlighted in the nomenclature section. Wall friction is neglected as the Reynolds numbers in problems of interest are very large. The aft-injected liquid spray is assumed to be monodisperse with a droplet size corresponding to its Sauter mean diameter. The gas phase composition is permitted to evolve in time and changes are reflected by vaporized and thermally-decomposed hydrogen peroxide. The specific heats of the decomposition products and of the hydrogen peroxide vapor are presumed to be constant in the analysis. The decomposition reaction is assumed to obey 1st order unimolecular reaction kinetics per the work of prior researchers [1-7]. Major model elements include basic mass balances, kinetics modeling, droplet dynamics, and control volume conservation laws. These elements are discussed in the following subsections.

Mass Balances

The relative slip between the phases creates significant issues in the analysis. Presume that at t=0 we begin with a collection of n_d droplets of initial diameter D_o. These droplets are accelerated and evaporated by the gas stream over a time t_v. The gases passing over the droplet cloud are assumed to be at the freestream conditions defined by the catalyst bed exhaust and the vapor emanating from the drops is presumed to be convected downstream at the velocity of the mixture. The distance traveled by the gas stream (x_{vg}) during this evaporation time can be estimated assuming constant gas velocity:

$$x_{vg} = v_{go} t_v \tag{1}$$

A control volume can be defined that includes the n_d droplets and the volume/mass of catalyst bed gases that interact with the droplet cloud during the time which it is evaporating. Figure 2 provides a schematic representation of this control volume. Assuming that the flow path is of constant cross-sectional area, A, the mass of catalyst bed exhaust that interacts with the evaporating cloud can be expressed:

$$m_{cat} = \dot{m}_{cat} t_v \tag{2}$$

Assuming a quasi-steady process with regard to the injection and bulk inflow of gases, the flowrate ratio between the liquid injectant and gas must be the same as the mass ratio in the selected control volume. Under this constraint, we may write:

$$\frac{m_d}{m_{cat}} = \frac{\dot{m}_l}{\dot{m}_{cat}} = \frac{n_d \rho_l \pi D_o^3}{6 m_{cat}} \tag{3}$$

Such that the number of droplets required to achieve the given flow split is then:

$$n_d = \frac{6 \dot{m}_l t_v}{\pi \rho_l D_0^3} \tag{4}$$

As the droplets evaporate, they will change the composition and mass of gas within the control volume. There will be a stratification of gas composition, pressure, and temperature as a result of the mixing of the vapor and the catalyst bed exhaust and from any decomposition reactions that occur during the time when the drops are evaporating. Droplets on the upwind side of the cloud will "see" catalyst bed exhaust conditions, while drops on the downstream side of the cloud will see cooled gases of different composition as a result of mixing of evaporant with the catbed gases. To address this stratification issue, we track the mean properties of the cloud and presume that the vaporization rate is controlled by the energy interchange with the bulk temperature/composition of the gases (both catbed and evaporant) within the control volume. To this end, we begin by computing the average composition of the gases in the control volume. Assuming that 90% hydrogen peroxide is decomposed in the catalyst bed, the decomposition reaction for this concentration can be written:

$$H_2O_2 + 0.210 H_2O \rightarrow 1.210 H_2O + \frac{1}{2} O_2$$

so that the initial mass of water and oxygen present in the control volume may be expressed:

$$m_{wo} = 0.424\, m_{cat}$$
$$m_{oo} = 0.526\, m_{cat} \tag{5}$$

Water is created via thermal decomposition of hydrogen peroxide vapor and from the portion of water evaporated from the 90% fluid assumed to be injected into the chamber. The resultant water flow can be expressed:

$$\dot{\delta}_w = 0.1\dot{\delta}_v - \frac{18}{34}\dot{\delta}_r \tag{6}$$

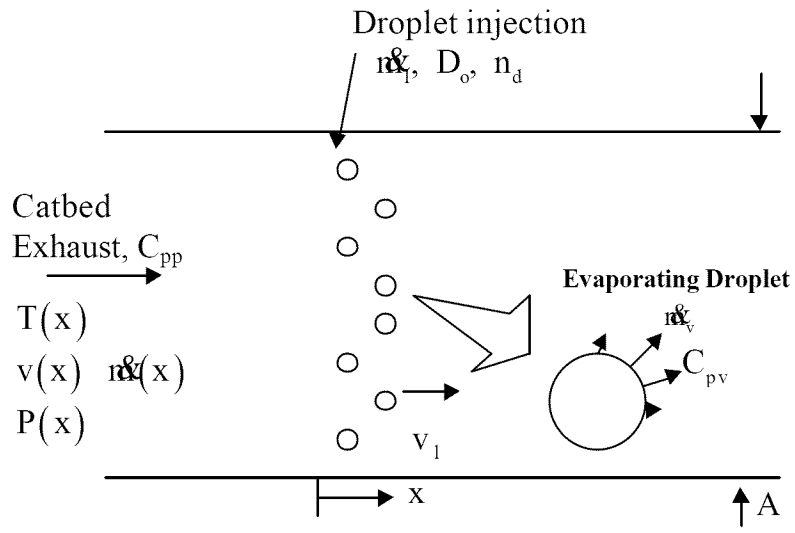

Figure 1: Definitions of variables/nomenclature associated with the model.

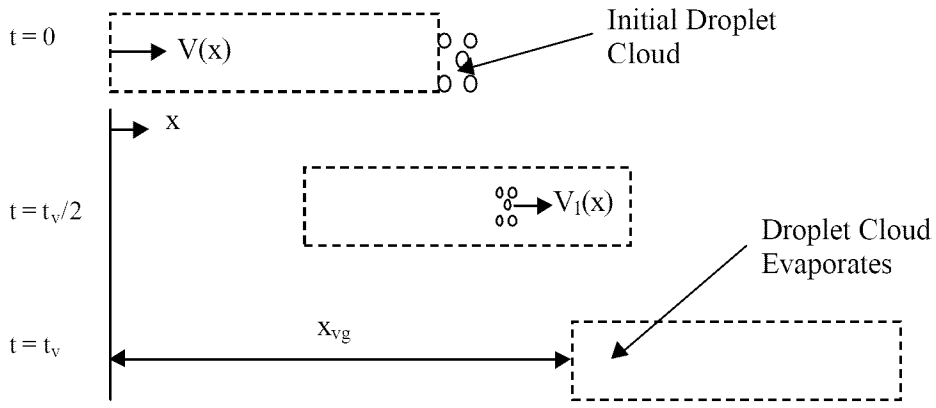

Figure 2: Definition of control volume of gas (indicated by the dashed lines) that is combined with given packet of liquid droplets over time interval t_v. The gas travels distance x_{vg} during the evaporation time.

where $\dot{m}_r$ is the rate of thermal decomposition of the evaporated peroxide gas (note that $\dot{m}_r$ will be a negative number). Similarly, the rate at which oxygen is created from the thermal decomposition reaction can be expressed:

$$\dot{m}_o = \frac{-16}{34}\dot{m}_r \tag{7}$$

Finally, the rate of net peroxide creation (assuming 90% HP in the drops) is:

$$\dot{m}_{HP} = 0.9\dot{m}_v + \dot{m}_r \tag{8}$$

where vaporization increases peroxide content and the decomposition reaction destroys HP in the control volume. Here we have assumed that the droplet evaporates uniformly in the sense that water is driven off at the equilibrium composition (10% of the droplet mass). In actuality, water is evaporated preferentially at least to some extent during the vaporization process. Since the vaporization process happens quickly in the cases of interest, we presume that this effect has only minor impact on results. Equations 6-8 can be integrated in time subject to the initial conditions given in Eq. 4 and the fact that $m_{HP0}=0$ (i.e. drops begin to evaporate at t=0). The vaporization and thermal decomposition rates appearing in Eqs. 6-8 are discussed in a subsequent section. Equations 6-8 are integrated using Huen's method [8] which is a second-order scheme based on trapezoidal integration.

Using the results of the mass integrations, the total gas mass in the control volume at any instant in time can be expressed:

$$m = m_w + m_o + m_{HP} \tag{9}$$

and the instantaneous mass fractions of each of the constituents can be computed:

$$\begin{aligned} y_w &= m_w/m \\ y_o &= m_o/m \\ y_{HP} &= m_{HP}/m \end{aligned} \tag{10}$$

Finally, the resultant molecular weight of the mixture W_{mix}, can be expressed in terms of the mass fractions and individual constituent molecular weights:

$$W_{mix}(x) = \frac{1}{\sum_{i=1}^{3} y_i/W_i} \tag{11}$$

Kinetics Model

The concentration of HP, C_{HP} , can be related to the mass fraction of HP present in the gases within the control volume [9]:

$$C_{HP} = y_{HP}\frac{PW_{mix}}{R_u T W_{HP}} \tag{12}$$

Now, the unimolecular kinetics reaction can be written:

$$\frac{dC_{HP}}{dt} = -KC_{HP} \tag{13}$$

where $K=A_o e^{-Ea/RuT}=K(x)$ in the present problem. Data from the literature [2,3] provide the following for the frequency factor and activation energy:

$$A_o = 10^{13}/\text{sec}$$
$$E_a = 48\frac{kcal}{mol}$$

Reference 10 provides a summary of prior kinetics studies for the interested reader. Combining Eq. (12) and (13) provides an expression for mass fraction of HP:

$$C_{HP}\left(\frac{1}{y_{HP}}\frac{dy_{HP}}{dt} + \frac{v}{P}\frac{dP}{dx} + \frac{1}{W_{mix}}\frac{dW_{mix}}{dt} - \frac{v}{T}\frac{dT}{dx}\right) = -KC_{HP}$$

or

$$\frac{dy_{HP}}{dt} = y_{HP}\left(-K - \frac{v}{P}\frac{dP}{dx} - \frac{1}{W_{mix}}\frac{dW_{mix}}{dt} + \frac{v}{T}\frac{dT}{dx}\right) \tag{14}$$

Here, we have transformed time derivatives to spatial derivatives for the pressure and temperature terms in Eq. 14. These fluid properties are assumed to correspond to bulk properties in the control volume and conservation of momentum and energy will ultimately be used to compute these terms (as shown in the following section). Since the fluid in the control volume is assumed to travel at the bulk gas velocity, v, the time increment is related to the spatial increment via dt = dx/v. Now, the mole fraction of hydrogen peroxide can be related to the mass of hydrogen peroxide and total mass in the control volume, $y_{HP} = m_{HP}/m_{cv}$, such that:

$$\frac{dy_{HP}}{dt} = y_{HP}\left(\frac{\dot{m}_{HP}}{m_{cv}} - \frac{\dot{m}_{cv}}{m_{cv}}\right) \tag{15}$$

So plugging Eq. (15) into Eq. (14) provides the rate of HP mass change with time due to decomposition reactions within the control volume:

$$\frac{dm_{HP}}{dt})_{kin} = \frac{dm_r}{dt} = m_{HP}\left[\frac{1}{m_{cv}}\frac{dm_{cv}}{dt} - K - \frac{v}{P}\frac{dP}{dx} - \frac{1}{W_{mix}}\frac{dW_{mix}}{dt} + \frac{v}{T}\frac{dT}{dx}\right] \quad (16)$$

Equation 16 describes the rate of gas decomposition due solely to kinetics effects. In our problem, we also have mass addition of HP vapor due to droplet vaporization (when drops are present). For a 90% peroxide drop undergoing non-preferential vaporization $\dot{m}_{HP} = 0.9\dot{m}_v$. We need to add this contribution to offset decreases in peroxide vapor flow due to decomposition. Adding this contribution to Eq. (16) we get:

$$\frac{dm_{HP}}{dt} = m_{HP}\left[\frac{1}{m_{cv}}\frac{dm_{cv}}{dt} - K - \frac{v}{P}\frac{dP}{dx} - \frac{1}{W_{mix}}\frac{dW_{mix}}{dt} + \frac{v}{T}\frac{dT}{dx}\right] + 0.9\dot{m}_v \quad (17)$$

Droplet Evaporation and Dynamics Model

The mass addition from vaporization can be computed using the simplified "D^2 law" model [9]:

$$\dot{m}_v = 2\pi\frac{k_l D}{C_{pv}}\ln(1+B_q) \quad (18)$$

where the k_l is liquid thermal conductivity and Spalding number B_q is defined:

$$B_q = C_{pv}\frac{(T - T_{sat})}{[h_v + C_{pl}(T_{sat} - T_l)]} \quad (19)$$

This parameter measures the ratio of the enthalpy driving the evaporation to the enthalpy required to evaporate the fluid in the drop. Since the gas temperature varies with time/space in this application, Eq. 18 must be integrated numerically and the droplet size history does not exactly correspond to a D^2 law behavior.

Considering the forces on an individual drop, we can determine its instantaneous acceleration:

$$\frac{dv_l}{dt} = \frac{A_d C_D \rho (v - v_l)^2}{2m_d} \quad (20)$$

where C_D is the drag coefficient, A_d is the projected area, and the mass of drop, m_d, is computed from the mass lost from vaporization at any instant in time:

$$m_d = m_{do} - \int_{t=0}^{t} \dot{m}_v dt \quad (21)$$

The instantaneous droplet diameter, D_d, and cross-sectional area, A_d, are computed assuming the drop remains spherical:

$$D_d = \sqrt[3]{\frac{6m_d}{\pi\rho_l}}$$
$$A_d = \frac{\pi}{4}[D(t)]^2 \quad (22)$$

As the droplet becomes vanishingly small, several of the drop characteristic equations above tend to diverge. For this reason, we choose a practical lower limit on the droplet mass in order to avoid numerical difficulties in integrating the equations beyond the point where drops vanish. Droplets are assumed to be completely vaporized when their mass is reduced to 0.1% of the initial droplet mass. This threshold provides adequate accuracy in mass, energy and momentum balances on the control volume.

Control Volume Conservation Laws

As mentioned previously, the control volume for the analysis is assumed to be the mass of gas that passes over a given packet of droplets. The size of the control volume is fundamentally set by the droplet vaporization time as noted in Eqs. 1-4. The properties of the gas within the two-phase mixture are computed assuming perfect mixing of all evaporated peroxide/water with the remaining gases within the control volume. This assumption allows one to compute the bulk properties of the mixture as a function of distance traveled by the gas. Furthermore, the average environment realized by droplets within the control volume is assumed to be represented by gas properties computed under this assumption as previously stated in the droplet dynamics discussion above. The momentum and energy balances on the control volume follow the approach of Shapiro [11]. The unsteady evolution of the two-phase flow is treated in a parabolic fashion wherein gas property changes are determined by a spatial stepping procedure along the length of the combustion chamber.

Energy interactions occur with the droplets via the opposing interactions of energy lost to vaporize the drops and energy gained from thermal decomposition. Kinetic energy interactions are small in the subsonic flows of interest, but are maintained for completeness. The initial thermal and kinetic energy entering an incremental control volume can be expressed:

$$(m_w + m_o) C_{pp} T + m_{HP} C_{pv} T + 0.5 m_v^2 \qquad (23)$$

Here m and v are the gas mixture mass and velocity, respectively and C_{pp} and C_{pv} are constant pressure specific heats of the decomposition products and HP vapor, respectively. The energy leaving the incremental control volume includes changes due to mass additions from vaporization, temperature changes, energy contributed to evaporated liquid, and energy liberated from the decomposition of HP vapor:

$$\begin{aligned}&(m_w + dm_w + m_o + dm_o) C_{pp} (T + dT) \\ &+ (m_{HP} + dm_{HP}) C_{pv} (T + dT) \\ &+ 0.5(m + dm)(v + dv)^2 + dm_v h_{lv} + dm_r h_{rxn}\end{aligned} \qquad (24)$$

where h_{lv} measures the energy required to heat the evaporated liquid to its saturation temperature, to vaporize it, and to superheat it to the local mixture temperature:

$$h_{lv} = C_{pv} (T - T_{sat}) + h_v + C_{pl} (T_{sat} - T_l) \qquad (25)$$

Here T_{sat} is the saturation temperature of the 90% HP, h_v is the heat of vaporization, and T_l is the liquid temperature at which the drops are injected. Equating Eqs. 23 and 24 and dividing both sides by the time increment dt provides the final form for the energy balance:

$$\frac{dT}{dt} = \frac{1}{m C_p} \left[\begin{array}{l} -\dot{m}_r h_{rxn} - ((\dot{m}_w + \dot{m}_o) C_{pp} + \dot{m}_{HP} C_{pv}) T \\ -\dot{m}_v h_{lv} - mv \dfrac{dv}{dt} - \dot{m}_v \dfrac{v^2}{2} \end{array} \right] \qquad (26)$$

where $mC_p = (m_w + m_o) C_{pp} + m_{HP} C_{pv}$. Initially, the temperature is set to the temperature of the catalyst bed exhaust to provide the condition for initiating integration of Eq. 26.

The gas pressure distribution in the combustion chamber can be determined from a momentum balance on the control volume. Pressure forces and drag on the droplets represent the two forces imposed on the fluid and momentum interactions also occur due to the mass addition from the vaporized fluid. The relevant differential form of the momentum equation can be expressed:

$$PA - (P + dP) A - dX = (\dot{m} + d\dot{m}_v)(v + dv) - \dot{m} v - v_l d\dot{m}_v$$

or

$$-A\,dP = dX + \dot{m}\,dv + v\,d\dot{m} - v_l\,d\dot{m}_v \qquad (27)$$

Here, the flowrate changes are entirely attributable to vaporization such that $d\dot{m} = d\dot{m}_v$. The net drag force on the droplet may be expressed:

$$X = C_D \frac{1}{2} \rho (v - v_l)^2 \frac{\pi}{4} D_d^2 \qquad (28)$$

Substituting Eq. 28 into Eq. 27 we obtain:

$$\frac{dP}{dx} = -\frac{dX}{dx} - \frac{\dot{m}}{A} \frac{dv}{dx} - \frac{(v - v_l)}{A} \frac{d\dot{m}_v}{dx} \qquad (29)$$

Using the fact that v = dx/dt, the derivative $d\dot{m}_l / dx = v\, d\dot{m}_l / dt$. The remaining derivatives on the right-hand side of Eq. 29 are determined from first-order upwind differencing. The initial pressure is an input to the model and the drops are assumed to enter with no axial component of velocity in computing their initial drag.

The gas density, ρ, is computed from P.G. law:

$$\rho = \frac{P W_{mix}}{R_u T} \qquad (30)$$

and the local gas velocity is computed from continuity equation:

$$v = \frac{\dot{m}}{\rho A} \qquad (31)$$

where A is the cross-sectional area of the combustion chamber.

Gas and Liquid Thermodynamic Properties

All gas and liquid thermodynamic properties for RGHP were taken from the Hydrogen Peroxide Handbook from Rocketdyne[12]. For the viscosity, liquid thermal conductivity, density, and vapor specific

heat fourth order curve fits were calculated from graphical data. Also, a specific curve fit was provided for the vapor pressure of 90% RGHP. Other parameters such as liquid specific heat, molecular weight, saturation temperature, binary diffusivity, activation energy, rate constant, and vapor thermal conductivity were taken as constant values over the entire decomposition process. All values used are listed in the table below.

Table 1: Constant Hydrogen Peroxide Properties Used

	Value	Units
Liquid Specific Heat, C_{pl}	0.663	Btu/lb R
Molecular Weight, 90% HP	31.3	lb/lb-mol
Saturation Temperature, T_{sat}	746.161	R
Binary Diffusivity	$5.2e^{-5}$	in^2/sec
Activation Energy, E_a	48,000	cal/mol
Rate Constant, A_o	10^{15}	sec^{-1}
Vapor Thermal Conductivity	0.0542	Btu/hr ft R

Solution Methodology

Time and spatial integrations are performed using a second-order trapezoidal integration scheme, Huen's method, as mentioned previously. The solution methodology for the scheme is as follows:

1. Input initial conditions including chamber diameter, catalyst bed flowrate, pressure, temperature, secondary liquid injection flowrate, droplet size, and known constants related to thermodynamic and kinetic properties of the mixture.
2. Input or guess a vaporization time, t_v.
3. Compute the number of droplets, initial catalyst bed gas, liquid, oxygen, and water vapor masses per Eqs. 2-5.
4. Compute/input the desired timestep and initialize the time to t=0.
5. Begin time stepping loop.
6. Compute current values of derivatives of control volume masses (Eqs. 6-8), reacted and vaporized masses (Eqs. 16-17), droplet temperature and velocity (Eqs. 18, 20), droplet mass and diameter (Eqs. 21, 22), gas temperature (Eq. 26) and pressure (Eq. 29), and current gas density and velocity (Eqs. 30, 31).
7. Compute predicted values at the new time level using Huen's method. For the equation dy/dt = f(x) we would define the predicted value at the new time level as $y^* = y_i + \Delta t\ (dy/dt)_i$ where the subscript "i" denotes the current time level and Δt denotes the timestep. Predicted values are computed for all dependent variables including masses, mass fractions, gas conditions, droplet size and mass, liquid temperature, gas and liquid properties at the new predicted temperature and pressure, gas and liquid velocities, and droplet drag.
8. Compute derivatives described in step 6 above at the new time level using the starred quantities computed in step 7. For example, we define $(dy/dt)^* = f(x^*)$ where x^* denotes the dependent variable as computed in step 7. The dy/dt^* value is the predicted slope of the function at the new time level.
9. Take a time step ($t = t+\Delta t$) and compute updated values for all dependent variables using Huen's method: $y_{i+1} = y_i + 0.5\,\Delta t\,[\ dt/dt|_i + dy/dt^*]$. Using this approach, update gas mass and composition, droplet mass, gas-phase properties, liquid temperature, and droplet size. If the droplet mass falls below the selected threshold value (0.1% of its initial mass), set a flag to eliminate computations involving droplets and set the droplet size to zero. Record the vaporization time, t_v, coincident with this event.
10. Return to step 5 until the desired number of timesteps are executed.
11. Compare the vaporization time computed in step 9 with the input value in step 2. Update vaporization time as required and perform steps 3-10 again. This process converges rapidly in 2-3 iterations such that the vaporization time remains unchanged for subsequent iterations.
12. Generate results once the converged solution is obtained.

Typically, 500-1000 timesteps are executed in a simulation. Grid function convergence studies have demonstrated that this resolution is sufficient to cause the solutions to be insensitive to the timestep. The model was programmed in a Matlab[13] script and runtime is on the order of a few seconds on a current generation personal computer.

Model Validation and Results

The model was validated against a series of experimental studies conducted at Purdue Univerity [14]. In these studies, 90% and 98% HP was injected downstream of a catalyst bed and the decomposition efficiency of the secondary injection was inferred from measured chamber pressures. Tests were conducted over a large range of secondary liquid injection percentages from 11 to 81% for chambers with characteristic lengths (L*) ranging from 24.5 to 54.5 inches. The overall efficiency (η_{tot}) was determined from measured chamber pressure data and presumed to be comprised of a weighted average of the efficiency of

the primary (η_p) and secondary (η_s) injectant efficiencies:

$$\eta_{tot} = x_s \eta_s + (1 - x_s)\eta_p \qquad (32)$$

where x_s is the ratio of secondary-to-primary massflows. Assuming that the catalyst bed is performing with perfect efficiency (η_p=1), the decomposition efficiency for the secondary stream was determined from measured chamber pressure.

The model was used to simulate this process inputting the theoretical catalyst bed conditions and using the measured chamber pressures. The model was run with the x_s value of interest and the integration was concluded at the entry to the nozzle throat section. At this location, the η_{tot} value was assumed to be equivalent to the ratio of the unreacted HP vapor (m_{HP}) to the local mass of gas in the control volume, m. Equation 32 was then used to compute the corresponding η_s value. The droplet size was adjusted to match experimental data at x_s=0.2, and the same drop size was then used for other x_s values to determine how well the model predicted the experimentally-observed trends.

Figure 3 summarizes the experimental and analytical decomposition efficiencies for secondary injection of 90% peroxide. Here, the liquid mass fraction is the ratio of secondary mass flow to total mass flow and this is plotted against the total percent of peroxide decomposition. A drop size of 100 microns, a reasonable value for a transverse jet injector as was used in the experiments, was assumed for all model simulations. Results show an excellent agreement over a wide range of liquid mass fraction values with the exception of the lone experimental data point at the very large flow split of 0.4. Figure 4 provides a similar comparison for the case where 98% fluid is used as the secondary injectant. Here, the best correlation with the more limited experimental results was obtained with a drop size of 135 microns. Since there is clearly a distribution of droplet sizes and the surface tension and density of the fluid do change somewhat from 90 to 98% concentration, there is good reason to expect that some adjustment in the drop size would be required in this case. Based on these encouraging results, the model was exercised over a broad range of conditions as summarized in the following section of the report.

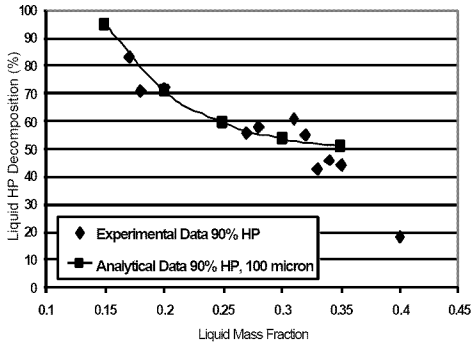

Figure 3: Comparison of Experimental Decomposition Efficiency Measurements [14] with Model Results for 90% HP Secondary Injection

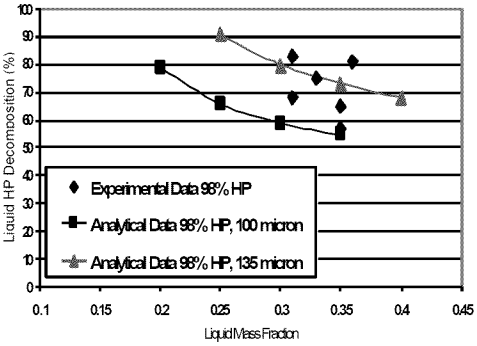

Figure 4: Comparison of Experimental Decomposition Efficiency Measurements [14] with Model Results for 98% HP Secondary Injection

A "baseline case" was created to assess the detailed behavior of the secondary injection process. Values for model inputs for this case are summarized in Table 2 below. A modest 5% secondary injection was selected for study and a typical catalyst bed flux of approximately 0.25 lb/s/in^2 was used in the simulations. Results from this case are summarized in Figs. 5-8. In Fig. 5, the gas properties, non-dimensionalized against their respective initial values, are plotted as a function of distance. The gas temperature drops initially due to the cooling effect of the droplet evaporation. As the thermal decomposition begins to take hold, the temperature increases and asymptotically approaches the initial catalyst bed exhaust temperature. Since the model assumes negligible heat losses outside the system, the decomposition temperature should eventually be attained. Slight differences were observed in some cases due to the effects of variable specific heats used in the

temperature integration. The minimum temperature attained in this baseline case corresponds to a 55 °K drop.

The pressure in the gas drops very slightly for this modest injection condition as the gas must give up momentum to accelerate the drops to the local mixture velocity. The gas velocity has an interesting trend; the initial decrease is due to the cooling effect of the evaporation process raising the gas density in the control volume and thereby decelerating the flow. The increase in the latter stages is attributed to the additional mass represented by the evaporated drops. Probably the most compelling result of the simulation is the axial distances required to achieve thermal decomposition for this baseline case of only 5% secondary injection.

Figure 6 compares gas and liquid velocities for the baseline conditions. The drops are accelerated to a velocity very near that of the gas as they vanish at an axial distance of about 13 inches from the injection point. Figure 7 shows the mass production rates for peroxide vapor, water, oxygen, and reacted fluid. Note that in this case, the peak reaction rates occur roughly midway through the drop evaporation process. The droplet size has a strong effect on this behavior as will be noted in following parametric studies. Figure 8 shows the actual masses of the three constituents in the mixture showing a peak peroxide concentration in the region where the reaction rate is also a maximum (maximum negative value).

Table 2: Input Parameters for Baseline Case

	Value	Units
Main Catbed Flow HP Concentration	90	%
Secondary Liquid HP Concentration	90	%
Main Catbed Mass Flow	0.2	lb/sec
Secondary Liquid Mass Flow (Percent of Main Flow)	5	%
Chamber Pressure	500	psi
Chamber Diameter	1.0	in
Initial Liquid HP Drop Diameter	100	micron
Initial Liquid Droplet Temperature	570	R

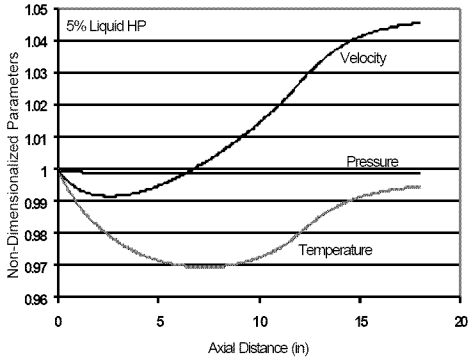

Figure 5: Non-Dimensional Pressure, Temperature, and Velocity for Baseline Case(Table 2) Secondary Injection Conditions

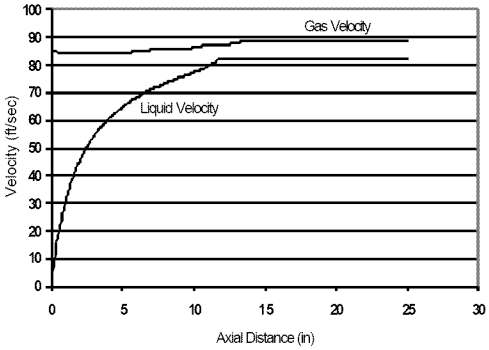

Figure 6: Gas and Liquid Velocities for Baseline Case (Table 2) Injection Conditions

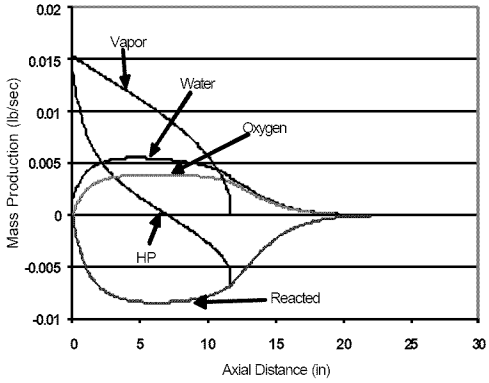

Figure 7: Mass Production Rates for Baseline Case (Table 2) Conditions

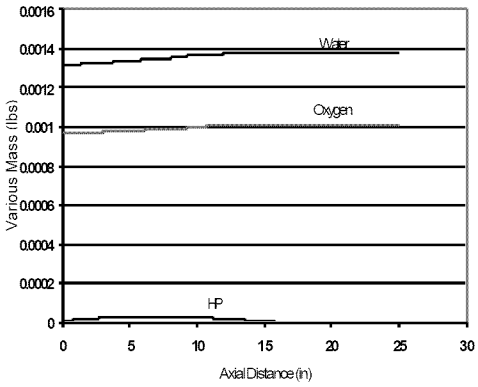

Figure 8: Control Volume Masses for Baseline Case (Table 2) Injection Conditions

The baseline case results are terribly depressing from the point that we are requiring 15-25 inches of chamber length to permit the vaporization and thermal decomposition process to complete itself even for this modest 5% injection condition. To assess the reason for this unfortunate behavior, consider an isothermal case in which peroxide vapor is decomposed at various fixed gas temperatures. In this case, the reaction rate, K, is constant and an analytic solution exists for the concentration of HP as a function of time:

$$\ln\left(\frac{C_{HP}}{C_{HPo}}\right) = -Kt$$

where C_{HPo} is the initial concentration of hydrogen peroxide vapor. We can define the half-life of this kinetic process, when $C_{HP}/C_{HPo}=1/2$ as:

$$t_{1/2} = \frac{\ln(2)}{K}$$

For the reaction activation energy and frequency factors provided in the Kinetics Model discussion, this half-life time is plotted as a function of temperature in Fig. 9. The right axis in Fig. 9 also shows the concentration of hydrogen peroxide consistent with an adiabatic decomposition temperature on the left axis. Figure 9 provides some compelling results that point to the heart of the decomposition physics in this problem. For 90% HP, the decomposition temperature is around 1850°K, and the corresponding half life time is roughly one millisecond. This implies that it takes about one millisecond to halve the concentration of HP vapor formed in a secondary injection process; a relatively long time given the fact that gases traverse the combustion chamber in a comparable time interval. Of course, if substantial cooling results from the secondary injection, the process will take even longer as K drops exponentially with temperature.

Readers should note the large sensitivity of the inherently exponential result. For temperature consistent with a 95% HP exhaust, the half-life time is decreased an order of magnitude to 0.1 msec. At bipropellant combustion temperatures, the decomposition process is literally measured on a microsecond timescale and is all but instantaneous in terms of the millisecond-level fluid mechanic-related times. While a negative result in terms of a classical thermal decomposition, Fig. 9 points to the incredible benefits that can be obtained by conducting the thermal decomposition at higher temperatures. Prior experience with hybrid rockets [15] running in the thermal decomposition mode have provided experimental confirmation of this result; i.e. extremely efficient decomposition (and the subsequent combustion) can be attained in reasonable length combustion chambers.

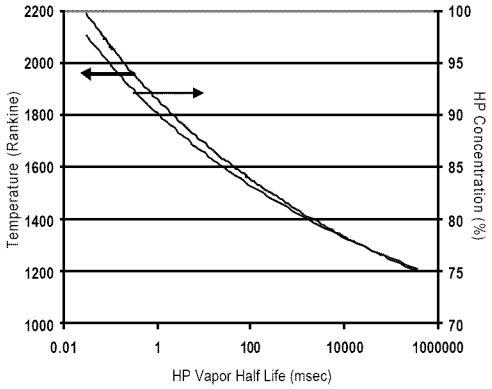

Figure 9: Half-Life Decomposition Time for Hydrogen Peroxide Vapor

Parametric Studies

While the prior results indicate great difficulties in achieving thermal decomposition of HP vapor in HP decomposition products, there is still much insight that can be obtained from conducting parametric studies with the model. Studies were conducted to independently assess the effects of varying the secondary liquid hydrogen peroxide mass flow, the initial drop diameter, the secondary liquid hydrogen peroxide concentration, the mass flux or gas velocity, and the droplet

temperature, respectively. The following section provides a summary of these studies.

Effect of Varying Secondary Liquid HP Mass Flow

The percentage of secondary liquid mass flow to main catbed flow was varied to analyze the effect on the thermal decomposition process. All other input variables remained fixed at the values shown in Table 2. Figure 10 depicts the resulting gas temperature distributions for various secondary liquid mass flow percentages of the main catbed flow. The point where the curve ends represents the calculated decomposition distance. One can note that for the 14% injection case, the liquid injection nearly freezes the peroxide vapor concentration as the temperature drop is severe enough to nearly eliminate the thermal decomposition mechanism. The reaction rate, K, drops from an initial value of over 600/sec at the 1850R temperature to 1.77/sec at the 1480K minimum temperature of the evaporatively-cooled gases. This dramatic reduction in reaction rate all but eliminates thermal decomposition.

Figures 11 and 12 present the effects of secondary injection level on gas pressures and velocities. Pressure drops increase with secondary injection as a larger amount of momentum exchange is required to accelerate the larger amounts of liquid, although overall drops in all cases are quite small. Gas velocities increase according to the larger variations in flow attendant to larger liquid injection fractions. Figure 13 summarizes the decomposition distance as a function of percent secondary liquid injection assuming threshold values signaling the end of the process at 1% or 5% of the original peroxide present within the liquid. The results are disheartening in that large distances are required even for modest levels of secondary injection. Finally, Table 3 gives the numerical data for calculated decomposition distance.

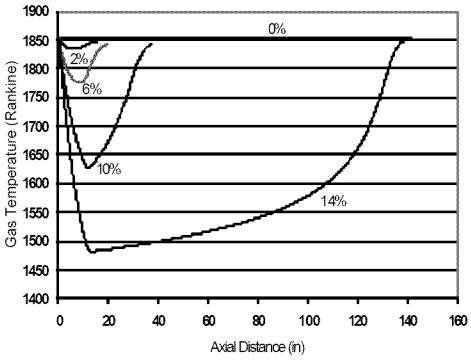

Figure 10: Effect of Percent Secondary Liquid Injection on Gas Temperature, 90% HP

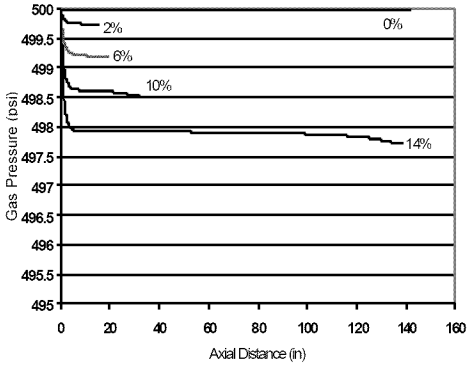

Figure 11: Effect of Percent Secondary Liquid Injection on Gas Pressure, 90% HP

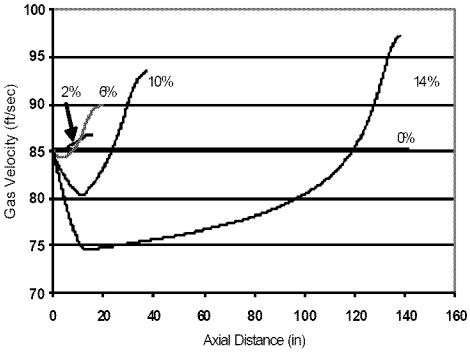

Figure 12: Effect of Percent Secondary Liquid Injection on Gas Velocity, 90% HP

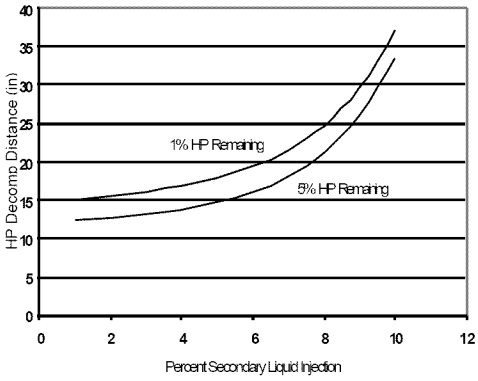

Figure 13: Effect of Percent Secondary Liquid Injection on Decomposition Distance assuming 1% or 5% of original HP remains

Table 3: Numerical Data for varying Percent Secondary Liquid Injection, 90% HP

% Injection	1% Remaining Decomp Distance (in)	5% Remaining Decomp Distance (in)
0	0	0
1	15.045	12.306
2	15.540	12.701
3	16.154	13.213
4	16.946	13.840
5	17.976	14.751
6	19.426	16.141
7	21.556	18.123
8	24.732	21.278
9	29.596	26.111
10	37.123	33.597
12	66.798	63.271
14	138.423	134.905
16	310.940	307.533

Effect of Initial Drop Diameter

Next, the effect of initial drop diameter was explored and the model was run for droplets ranging from 50 to 600 microns. All other inputs were maintained at the values provided in Table 2. The range of sizes considered gave very large ranges of decomposition distances, for this reason results are summarized for smaller and larger drops in Figs. 14 and 15, respectively. For small drops, the process tends to be kinetics limited, i.e. very little decomposition occurs during the vaporization event due to its speed and the large amount of cooling occurring in this case. The larger drops show the opposite trend of being essentially vaporization limited in that the decomposition kinetics essentially keep the local vapor content very low as a result of the increased vaporization time. This result indicates some prospects of managing thermal decomposition processes using larger drops or lower evaporation rates. If a vertical structure can be created to enhance droplet lifetimes in a given chamber, then it may be possible to keep temperatures high enough to get efficient thermal decomposition. Figure 16 summarizes the resulting decomposition distances based on ending criteria of either 1% or 5% of the original peroxide present. Despite the deleterious effects of large evaporative cooling, the smaller drops still maintain shorter decomposition lengths than the larger drops for the configuration studied. Table 4 contains the numerical data for droplet diameter variation.

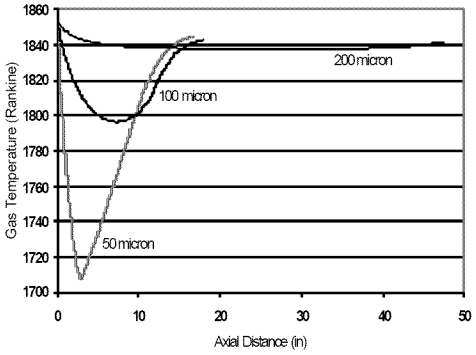

Figure 14: Effect of Initial Droplet Diameter on Gas Temperature (50-200 micron)

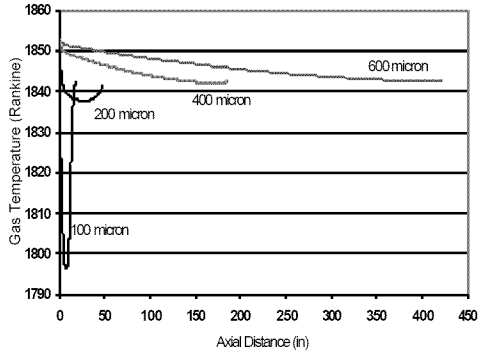

Figure 15: Effect of Initial Droplet Diameter on Gas Temperature (100-600 micron)

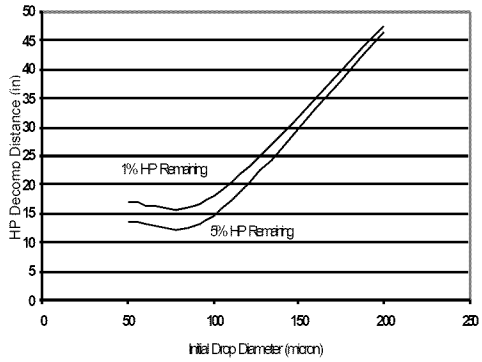

Figure 16: Effect of Initial Droplet Diameter on Decomposition Distance assuming 1% or 5% of original HP remains

Table 4: Numerical Data for varying Initial Droplet Diameter, 90% HP

Diameter (micron)	1% Remaining Decomp Distance (in)	5% Remaining Decomp Distance (in)
50	16.778	13.646
100	17.976	14.751
200	47.423	46.708
400	186.734	186.734
600	422.302	422.302

Effect of Secondary Liquid Hydrogen Peroxide Concentration

It was discovered that values of peroxide concentration below 90% produce unacceptably large decomposition distances in the cases discussed above. While silver-based catalyst beds cannot operate using 98% fluid, it would be feasible to aft-inject this fluid to increase energy content and promote more rapid decomposition. A study was conducted on this basis at various injection fractions with other input parameters fixed at values shown in Table 2. Figure 17 depicts the effect of percent secondary liquid injection on gas temperature for various injection fractions. As in the 90% injection case (Fig. 10), the decomposition distance increases drastically when evaporative cooling drives gas temperatures below 1500 °R. Final temperatures exceed the initial values in this case due to the additional energy release in the decomposition of the 98% fluid. Figures 18 and 19 show the effect of gas pressure and velocity for 98% liquid peroxide with trends quite comparable to the 90% injection results. Figure 20 provides the resulting decomposition distances assuming 1% or 5% of the original peroxide remains and Figure 21 compares decomposition distances of 90% and 98% assuming 1% of the original peroxide remains. Substantial benefits in the reduction of decomposition distance can be achieved using 98% fluid. Finally, Table 5 provides the numerical data for decomposition distances.

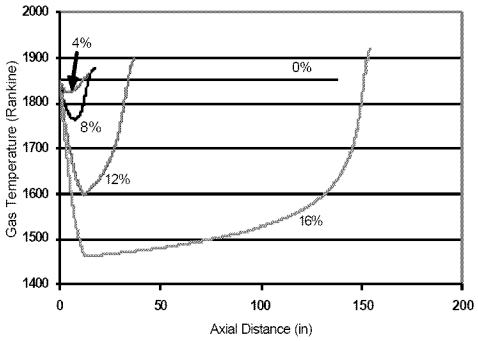

Figure 17: Effect of Percent Secondary Liquid Injection on Gas Temperature, 98% HP

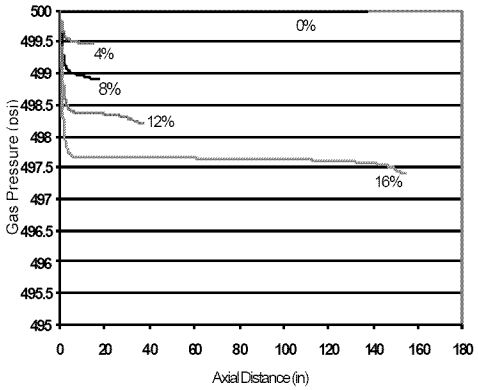

Figure 18: Effect of Percent Secondary Liquid Injection on Gas Pressure, 98% HP

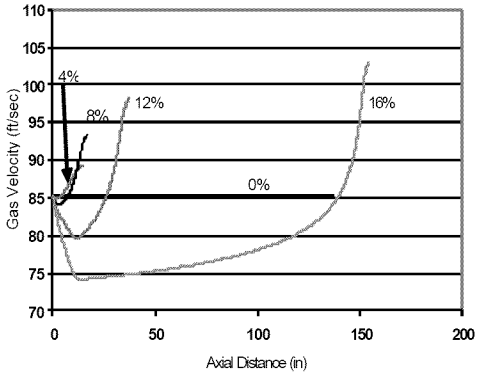

Figure 19: Effect of Percent Secondary Liquid Injection on Gas Velocity, 98% HP

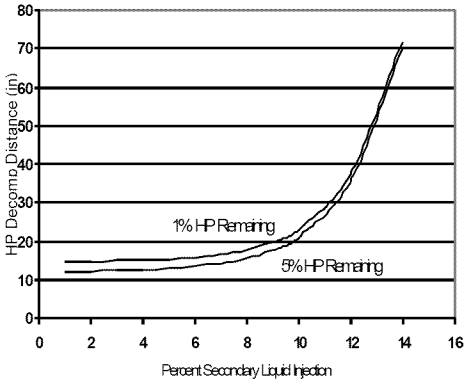

Figure 20: Effect of 98% Secondary Liquid on Decomposition Distance assuming 1% or 5% of original HP remains

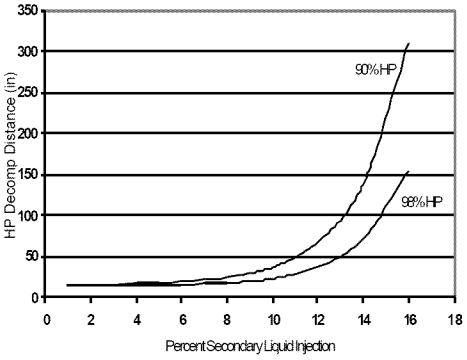

Figure 21: Effect of 90% and 98% Secondary Liquid on Decomposition Distance assuming 1% of original HP remains

Table 5: Numerical Data for varying Percent Secondary Liquid Injection, 98% HP

% Injection	1% Remaining Decomp Distance (in)	5% Remaining Decomp Distance (in)
0	0	0
1	14.673	12.098
2	14.794	12.297
3	14.909	12.435
4	15.135	12.684
5	15.403	13.029
6	15.839	13.485
7	16.493	14.278
8	17.737	15.532
9	19.758	17.618
10	23.133	21.065
12	37.258	35.410
14	71.830	70.175
16	154.352	152.752
18	346.637	345.290

Effect of Catalyst Bed Mass Flux or Gas Velocity

The mass flux (G) was varied by changing the chamber diameter which gave a mass flux range of approximately 0.15 to 1.0 lb/in^{2}sec. Figures 22, 23, and 24 show the resulting temperature, pressure, and velocity changes, respectively. Other inputs were maintained at the values shown in Table 2. Increasing mass flux basically increases gas velocity and stretches the axial coordinate accordingly. The higher velocities do create larger pressure drops (Fig. 23) since the momentum losses scale as ρv^2. The scaling of gas velocities with mass flux is shown in Fig. 24. The fact that increased mass flux essentially leads to a stretching of the axial distance (i.e. events still occur over the same time interval) leads to a nearly linear relationship between decomposition distance and mass flux shown in Figure 25. Table 6 provides the numerical data.

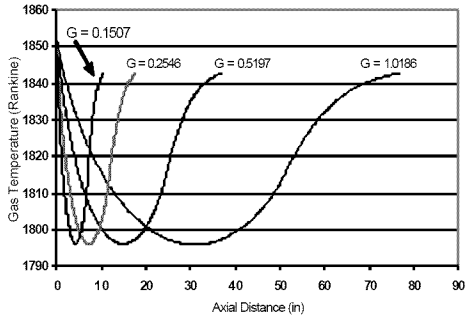

Figure 22: Effect of Mass Flux on Gas Temperature, 90% HP

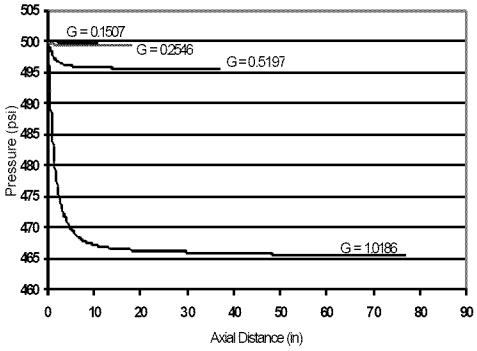

Figure 23: Effect of Mass Flux on Gas Pressure, 90% HP

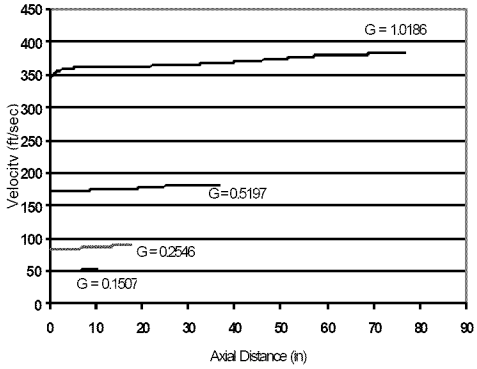

Figure 24: Effect of Mass Flux on Gas Velocity, 90% HP

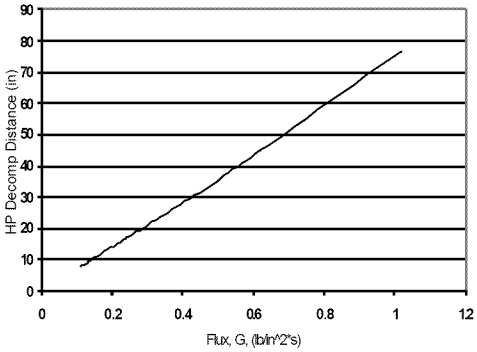

Figure 25: Effect of Mass Flux on Decomposition Distance assuming 1% of original HP remains

Table 6: Numerical Data for varying Mass Flux, 90% HP

Mass Flux (lb/in^2sec)	Chamber Diameter (in)	1% Remaining Decomp Distance (in)
1.0186	0.5	76.907
0.5197	0.7	36.946
0.3144	0.9	22.213
0.2546	1.0	17.976
0.2105	1.1	14.849
0.1507	1.3	10.627
0.1132	1.5	7.98

Effect of Injected Liquid Temperature

Some power cycles utilize the peroxide as a coolant prior to injection into the thrust chamber; for this reason, the effect of injectant temperature was investigated assuming remaining inputs remained at values shown in Table 2. Evaporation rates increase and gas subcooling effects decrease with increased liquid injectant temperature as noted in Fig. 26. The overall decomposition distance decreases accordingly as injectant temperature increases as summarized in Fig. 27 for the 1% threshold indicating the decomposition length. Table 7 gives the numerical data.

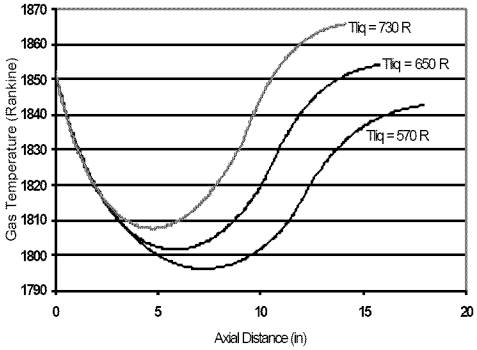

Figure 26: Effect of Droplet Temperature on Gas Temperature, 90% HP

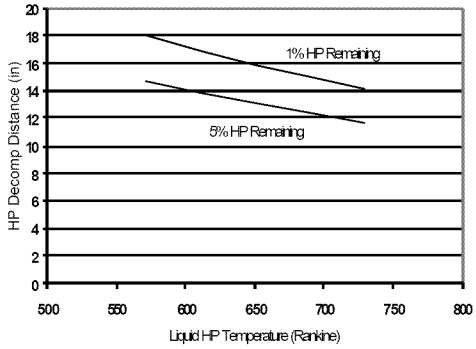

Figure 27: Effect of Droplet Temperature on Decomposition Distance assuming 1% or 5% of original HP remains

Table 7: Numerical Data for varying Droplet Temperature, 90% HP

Tliq (Rankine)	1% Remaining Decomp Distance (in)	5% Remaining Decomp Distance (in)
570	17.976	14.751
650	15.836	13.051
730	14.096	11.674

Conclusions

A one-dimensional model has been created to simulate the vapor-phase decomposition of hydrogen peroxide in a gas stream composed of HP decomposition products. The tool includes the effects of the finite-rate vapor phase kinetics, droplet evaporation and drag, and local gas temperature and pressure, and can be used for arbitrary HP concentrations in both main and secondary injectant streams. A single droplet size representative of the Sauter Mean Diameter of the parent spray is assumed in the integration. By adjusting this single parameter, excellent agreement is shown with measured data [14] for the case of 90% HP injectant and main flows.

A baseline case was selected to investigate 5% secondary injection of 90% HP into a 90% HP exhaust with a modest catalyst bed loading near 0.25 lb/in^2-s. A 100 micron initial drop diameter was selected based on results from validation studies. The performance of the secondary injection for this case is disheartening in that reaction lengths on the order of 18 inches are required even for this case of a fairly modest 5% secondary injection. The source of the problem was tracked to the kinetic half life of the vapor-phase decomposition process. The half-life is on the order of milliseconds for temperatures consistent with 90% HP decomposition, but drops rapidly to microsecond levels at bipropellant combustion temperatures. This unfortunate condition limits the appeal of thermal decomposition for monopropellant applications, although at higher concentrations more reasonable reaction distances are obtained.

The amount of secondary injection had strong effects on decomposition distance as the evaporative cooling effect nearly quenches the thermal decomposition reaction at higher secondary injection rates. The initial droplet size also had profound effects on the decomposition process. For very small drops (less than 100 microns), the process is inherently kinetics controlled, with large amounts of evaporative cooling taking place before significant vapor phase decomposition occurs. For large drops (greater than 200 micron), the process is inherently vaporization-limited as the decomposition keeps up reasonably well with the evaporation rates. Even though the cooling effects lengthen the process, the smaller drops still had shorter decomposition lengths. There may be mechanisms to utilize larger drops and maintain gas temperature if novel strategies can be devised to increase chamber residence times.

Simulations were also conducted using 98% fluid as the secondary injectant. The increased energy of these drops did improve results somewhat, but reaction lengths were still too long to be of use in practical combustors for aerospace applications. Increasing the temperature of the injectant also had beneficial effects. Increasing the chamber velocities or catalyst bed mass fluxes essentially led to proportional increases in reaction lengths, i.e. reaction times remained about the same.

Acknowledgements

This research was funded by a Phase I STTR awarded to IN Space, LLC and Purdue University by the Missile Defense Agency.

The authors would like to thank Purdue graduate students J.S. Mok and Nick Pearson for supplying previous experimental and analytical data for the decomposition of hydrogen peroxide.

References

1. Giguere, P.A., "The Thermal Decomposition of Hydrogen Peroxide Vapor II", Canadian J. of Chemistry, V25, pp. 135-150, 1947.
2. Giguere, P.A. and Liu, I. D., "Kinetics of the Thermal Decomposition of Hydrogen Peroxide Vapor", Canadian J. of Chemistry, V35, pp 283-293, 1957.

3. Satterfield, C. N., and Stein, T. W., "Homogeneous Decomposition of Hydrogen Peroxide Vapor", J. of Physical Chemistry, V61, 1957.
4. McLane, C.K. "Hydrogen Peroxide in the Thermal Hydrogen Oxygen Reaction I. Thermal Decomposition", J. of Chemical Physics, V17, 1949.
5. Conway, D.C., "Mechanism of the Homogeneous Decomposition of Hydrogen Peroxide", J. of Physical Chemistry, V61, 1957.
6. Hoare, D.E., Protheroe, J.B., and Walsh, A.D., "The Thermal Decomposition of Hydrogen Peroxide Vapour", Transactions of the Faraday Society, V55, 1959.
7. Baldwin, R.R., and Brattan, D., "Homogeneous Gas-Phase Decomposition of Hydrogen Peroxide, 8th Intl. Symposium on Combustion, Pasadena California, 1960.
8. Hoffman, Joe D., Numerical Methods for Engineers and Scientists, 2nd Edition, Marcel Dekker, Inc., 1992.
9. Turns, Stephen R., An Introduction to Combustion, 2nd Edition, McGraw-Hill, 1996.
10. Pearson, N., Pourpoint, T., and Anderson, W. E., "Vaporization and Decomposition of Hydrogen Peroxide Drops", AIAA-2003-4642, AIAA Joint Propulsion Conference, Huntsville, AL, 2003.
11. Shapiro, Howard N. and Moran, Michael J., Fundamentals of Engineering Thermo-dynamics, 3rd Edition, John Wiley & Sons, 1996.
12. Hydrogen Peroxide Handbook, Chemical and Materials Sciences Dept., Rocketdyne, Canoga Park, CA, July 1967.
13. MATLAB 6.5 software program
14. Mok, J.-S., Helms, J., and Anderson, W., "Decomposition and Vaporization Studies of Hydrogen Peroxide," AIAA-2002-4028, AIAA Joint Propulsion Conference, Indianapolis, IN, July 8-10, 2002.
15. Wernimont, E.J., and Heister, S.D., "Combustion Experiments in a Hydrogen Peroxide/Polyethylene Hybrid Rocket with Catalytic Ignition," *Journal of Propulsion and Power*, V. 16, No. 2, pp. 318-326, 2000.